ARTICLE Open Access

Developing elastic foamed TPU fibers for dynamically daytime radiative cooling textile with buoyancy function

Yushu Wang 61, Hanyi Huang 61, Zeling Wang 61 and Wentao Zhai 61,2

Abstract

Porous materials are widely used in various scenarios due to their advantages such as good thermal insulation, flexibility, and ultra-lightness. Foaming technology has given porous materials more application areas by introducing uniformly distributed cellular structures into the polymer collective. In the past decade, we have conducted systematic studies around the preparation of multi-component polymer microporous materials and functional applications of porous materials. In this work, we propose the preparation of foamed TPU fibers and foamed fabrics (FT-fabric) with anisotropic cell structure using TPU as substrate by micro-extrusion foaming techniques. Thanks to the multistage cell distribution of the FT-fabric and the vibrational absorption of the polymer in the MIR band, the prepared FT-fabric has a near-infrared reflectance of >97%, which enables effective radiative cooling. The porous structure of the FT-fabric endows it with an ultra-low density, which is able to provide additional buoyancy in water. As a conceptual demonstration, FT-fabric is able to function as a cooling and buoyancy support in seaside scenarios, among other functions, providing a viable avenue for new functional garments.

Introduction

Polymeric foams with closed-cells and open-cells have the characteristics of lightweight and multiple functions, and have been widely used in various fields such as aerospace, automobiles, windmill blades, 5 G station, sports protection, construction, water treatment^{1–3}. The endowed air within closed cells gives polymeric foams with low density, thermal insulation, cushioning and low dielectric properties^{4,5}, while the multi-channel structure and capillary effect of open-cell structure endows polymeric foam with separation, filtration, sound absorption and liquid adsorption properties^{6,7}. Unfortunately, the traditional foaming techniques often use nonenvironmental friendly blowing agent or involve the use of large amounts of solvents, which is difficult to meet the development goals of carbon peaking and carbon neutrality.

Supercritical CO2 and N2 fluids are green and residuefree physical blowing agent, and has been used to fabricate microcellular polymers. Microcellular polymers have cell size of ~1-100 µm and cell densities of 10⁶⁻¹² cells/cm³ 8,9, and present much better mechanical properties in relative to the traditional polymeric foams with cell size larger than 100 µm. The microcellular foaming process contains the formation of homogeneous polymer/fluid system under high pressure and bubble nucleation induced by phase-separation of polymer/gas via heating or pressure quenching. The nucleated bubbles gradually increase in the process of fluid diffusion to form polymer foams with microcellular or even nanocellular structure 10-12. Continuous extrusion foaming, injection molding foaming, and batch foaming are three critical foaming methods to fabricate microcellular polymers, and among of them, the batch process is most popular, since its processing parameters and equipment are easily control. In the past 10 years, our group have developed various foaming technologies based on the batch process to fabricate bead foam¹³, foamed blocker¹⁴, foamed film^{15,16}, and 3D shaped foams^{17,18}, and various polymer systems

Correspondence: Wentao Zhai (zhaiwt3@mail.sysu.edu.cn)

© The Author(s) 2025

Open Access This article is licensed under a Creative Commons Attribution 4.0 International License, which permits use, sharing, adaptation, distribution and reproduction in any medium or format, as long as you give appropriate credit to the original author(s) and the source, provide a link to the Creative Commons licence, and indicate if changes were made. The images or other third party material in this article are included in the article's Creative Commons licence, unless indicated otherwise in a credit line to the material. If material is not included in the article's Creative Commons licence and your intended use is not permitted by statutory regulation or exceeds the permitted use, you will need to obtain permission directly from the copyright holder. To view a copy of this licence, visit http://creativecommons.org/licenses/by/4.0/.

¹School of Materials Science and Engineering, Sun Yat-sen University, Guangzhou, Guangdong Province, China

²Nanchang Research Institute, Sun Yat-sen University, Nanchang, China

such thermoplastic elastomers¹⁹, biodegradable plastics^{14,20}, high-performance plastics²¹ are used, and some technologies have been commercially used in running shoes and chemical mechanical polishing applications³.

Fiber materials, as one of the oldest and most basic materials, occupy an important position in the course of human development^{22,23}. In addition to the use of natural fibers, with the rapid development of synthetic fiber industry, fiber materials with special properties continue to come out, and its application has gradually expanded from the traditional clothing field to aerospace, environmental energy, biomedical and other high-tech fields, becoming an important foundation and strategic materials for the development of national economy and national defense military industry^{24,25}. As a new type of fiber material, porous fiber has been widely concerned because of its high porosity, low density and excellent thermal insulation properties, and is regarded as an effective thermal insulation fiber, which is expected to subvert down and replace microfiber, and has important application prospects^{26,27}. At present, most of the techniques for preparing porous fibers are ice crystal stencil method²⁸, phase separation^{29,30} and directional etching^{31,32}. Although these methods have successfully prepared porous fibers, they are faced with challenges such as insufficient strength, single function, complex preparation process, and difficult to accurately control cell structure, which greatly limits the practical application of porous fibers.

Supercritical fluid physical foaming technologies have been widely developed and used for the manufacture of foamed bulk materials, but there is very few research on the introduction of foaming technology into the field of fibers³³. Because of the rapid escape of blowing agent out of small diameter of fibers, it is difficult to achieve the foamed structure within fiber matrix during the foaming process. In recent studies, our group has developed micro-extrusion foaming technology to prepare the plastic porous fiber^{27,34}, where the plastic filaments are saturated by compressed CO2 or N2, and the saturated filaments are micro-extruded by a home-designed device into thin and foamed polymer melt. Through control of the residence time of foamed polymer melt, the cell structure can be adjusted within the 0.2-0.5 µm-sized porous fibers. Unfortunately, the plastic-based foamed fiber is brittle, and cannot reach the flexibility of existing fiber materials.

The reason why the foamed fiber has been widely concerned is that, in addition to the well-known advantages of heat insulation and ultra-lightweight. The ultra-wideband control of thermal radiation can be realized by adjusting chemical structure and cell structure of foamed fiber³⁵, and fiber's shape and distribution^{36,37}, and thus the thermal management strategy of heat insulation and

cooling can be realized³⁸. In the field of clothing or wearable devices, the application of porous fibers can effectively regulate the heat transfer between the human body and the external environment, and achieve reasonable control of human temperature^{39,40}. In addition, the cell structure endows porous fibers with ultra-light density, and swimsuit woven based on porous fibers can supply additional buoyancy in water, and further fiber modification such as UV resistance gives the porous fibers many advantages.

In this work, a TPU-based elastic and lightweight foamed fiber was prepared by the micro-extrusion physical foaming with using supercritical N_2 as a physical blowing agent. It was interesting to find that the asprepared foamed fiber presented excellent radiation cooling ability and lower density than seawater. The potential usage of the weaved porous fabrics in the scene of summer seaside was examined. The influences of cell structure on the infrared radiation's reflection and absorption of fabrics, and the buoyancy of swimwear fabric were discussed. Due to the scale of micro-extrusion physical foaming process, the developed elastic foamed fiber in this work has the prospect of mass production, and can be used in high-tech functional clothing.

Results and discussion Design strategy and fabrication

In this paper, the porous elastic TPU fibers were prepared by micro-extrusion foaming method, and the micro-extrusion foaming process is shown in Schematic Fig. 1a. N₂ was selected as the green physical blowing agent due to its low gas desorption rate, and the saturated N₂ with pressure of 25 MPa was applied, and a N₂ solubility of 1.25 wt% was obtained in the saturated TPU filament. The preparation of foamed fibers can be divided into three steps, including (1) gas saturation of TPU filament, (2) micro-extrusion of gas-saturated TPU filament, (3) collection of porous TPU fiber under stretching. During the micro-extrusion foaming process, the N₂saturated TPU filament was passed through the microextruder and then across the nozzle, the heating-induced cell nucleation occurred within the micro-extruder, and the gas-diffusion driven cell growth. Once the foamed polymer/gas melt was extruded out of the nozzle and then across the heating channel, the foamed melt was solidified and the formed cell structure was stabilized by air cooling. By adjusting the residence time of foamed polymer/gas melt within the extruder and the stretching degree of foamed fiber within the heating channel, the cell morphology of foamed fiber could be adjusted. The fabric (FT-fabric) obtained by knitting the as-prepared foamed fibers through a knitting machine has the advantages of ultra-low density, high elasticity, and porosity, which can

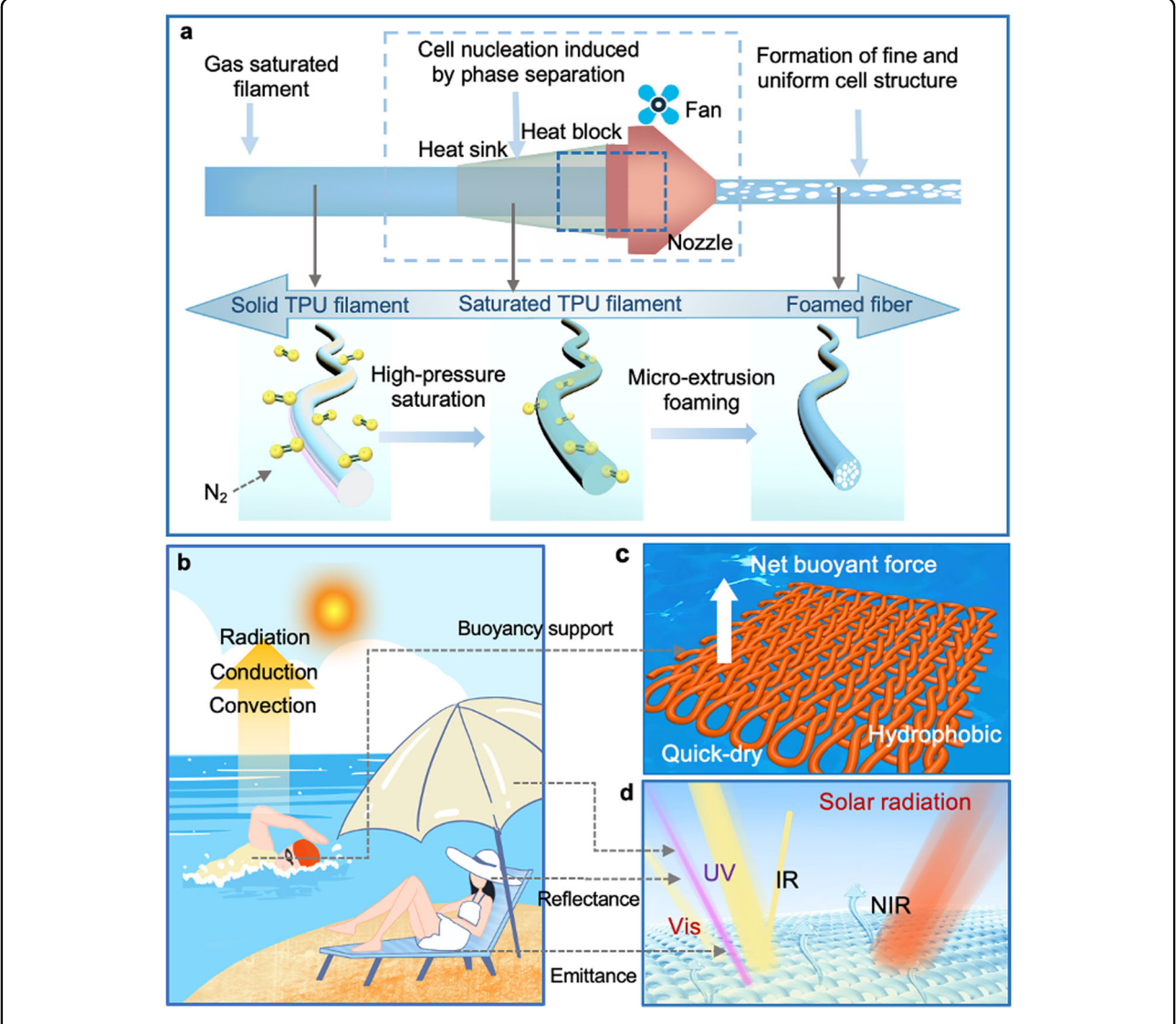


Fig. 1 Preparation and mechanism of FT-fabric. a Schematic diagram of preparation of micro-extruded foamed fiber. **b** Application diagram of FT-fabric. **c** Schematic diagram of radiant cooling of FT-Fabric. **d** FT-fabric water application diagram.

be used as a wearable device to achieve apparel applications⁴¹.

As shown in Fig. 1b, in a seaside environment with intense solar radiation, people often need to be protected by sun hats, sun umbrellas, and sunproof clothes, etc. Meanwhile, except for the solar radiation from the sun in the sky, the thermal radiation reflected by the ground cannot be ignored, which could constantly heat things on the ground 42,43. Therefore, in addition to block the sun, the selection of materials with a certain cooling function can help people maintain thermal comfortable in the hot environment 44. In the outdoor seashore, the acidity and alkalinity of seawater, corrosive, the radiation intensity of the sea surface, wind, waves etc. will have an impact on the comfort and safety

of the human body. Therefore, in the such complex environment want to improve human comfort, need the functionality of a more adequate and comprehensive functional clothing. The foamed fabric is able to effectively reflect solar radiation, block UV damage and nearinfrared heating, while have high emissivity within the atmospheric window (8–13 μm), which has an obvious role in regulating body temperature and keeping the body thermally comfortable (Fig. 1c). In addition, as shown in Fig. 1d, due to its ultra-low density, excellent chlorine resistance, UV resistance, hydrophobicity, FT-fabric can be worn as a swimming costume in seawater to provide a certain buoyancy for the human body in the water while drying quickly to ensure the human body's comfort after going ashore.

Physical properties of foamed fiber and FT-fabric

As shown in Fig. 2a, during the micro-extruded foaming process, the cell nucleation is induced via a rapid heating and the cell growth is enhanced by gas diffusion in microextruder at a fixed temperature, thereby forming a porous structure inside the TPU filament. In the fiber profile section (Fig. 2b), the dense and irregular porous structure is formed inside the fiber (Fig. S1). Compared with the common freeze-drying or phase separation methods, the cell structure formed by the micro-extruded foaming is in a more regular elliptical shape, with a smaller diameter and a tighter structure, and the cavities and micropores are also contracted. In order to achieve the application of foamed fibers for garments, we prepared them using a knitting flat knitting machine, the structure of which is shown in Fig. 2c. The woven foamed fibers can form a complete, dense tissue structure for functional applications.

We counted the cross-section, profile-section of the foamed fiber, and the pore size distribution of the knitted fabric. It can be seen that in the cross-section, the prepared foamed fibers have a pore size distribution in the interval of $0.5-15 \mu m$, and the wide distributions of nanopores and micropores are ~579 nm and ~8.5 μm, respectively (Fig. 2d). As for the profile-section, the fiber had a multiscale disordered porous structure with a porosity of ~83.2%, and the distribution of pore sizes extended to the range of 2-20 µm (Fig. 2e). In contrast, after weaving the foamed fibers, the pore distribution between fibers and fibers was in the range of 15-60 µm (Fig. 2f). It can be seen that FT-fabric has a large range of pore size distribution between 0.5 and 60 µm compared to ordinary textile materials. Among them, the size of the pore size in the fiber is comparable to the wavelength of sunlight (0.3~2.5 μm), which scatters sunlight more strongly. The interval of major pore sizes is also much smaller than the infrared wavelengths (7–14 μm), so the FT-fabric is transparent in the mid and far-infrared ranges and is able to emit the heat of the material without blocking the infrared emission from the human body. As can be seen in Fig. 2g, the foamed fiber prepared in this work is expected to achieve large-scale production due to simple preparation method, which is capable of stable high-volume preparation. Moreover, the foamed yarn has good wearable performance, which can achieve large-area fabric preparation by upper loom weaving (Fig. 2h). In addition, the tensile stress-strain curves of FT-fabric, sunproof cloth and swimwear were tested in Fig. 2i. FTfabric also showed a strength significantly higher than that of swimwear and close to that of commercial sunproof cloth. The results indicate that the prepared FTfabric has excellent mechanical properties and is easy to weave into functional textiles. Therefore, FT-fabric has great potential as a wearable device due to its excellent optical and mechanical properties.

Radiation cooling properties

The spectral properties of the FT-fabric and T-fabric before and after foaming were quantitatively characterized in the solar (0.5-2.5 µm) and AMI bands $(3-25 \mu m)$ (Fig. 3a). It can be seen that FT-fabric is able to achieve >97% solar reflection in the NIR band and exhibits high emissivity in the atmospheric window band $(8-13 \,\mu\text{m})$. This is due to the randomly distributed disordered holes inside the fibers after foaming that help to scatter sunlight, the scattering of sunlight is shown schematically in Fig. 3b. In contrast to conventional foamed fibers with orderly distribution and regular shape, foamed fibers contain small holes comparable to the wavelength of the short solar radiation as well as large holes comparable in the atmospheric window band. According to the Mie scattering theory⁴⁵, the cell size distribution close to the band has a strong solar reflectivity, and when the size is far away from the MIR band, it leads to a lower Mie scattering efficiency in the band, and in the non-window MIR band is conducive to a higher transmittance rate of the human body radiation, and achieves the effect of radiation cooling. In addition, it is well known that the emission and transmission of polymeric materials in the MIR region (the main human radiation band) is essentially dependent on their molecular bonds and functional groups, which have different vibrational absorption and emission characteristics in different band ranges. The presence and absence of strong molecular vibrations is a necessary prerequisite for high emission and transmission in the corresponding bands. For an ideal radiation-cooling textile, the vibrational absorption and emission frequencies of molecular bonds and functional groups should be limited to the MIR band (8–13 μ m). In Fig. 3c, we tested the FTIR-ATR curves of FT-fabric and T-fabric to characterize the transmittance, the transmittance of FT-fabric in the middle infrared band of 9-12 µm is lower than that of T-fabric. The transmittance tends to be about 1, and the sample tends to be about transparent because the T-fabric is not foamed, so transparency is high. On the contrary, the porous structure inside FT-fabric will reflect the incident light for many times to limiting its optical activity. The obvious transmittance decline of FT-fabric in the mid-infrared band can be attributed to: Firstly, the vibration absorption and emission frequencies of the molecular bonds and functional groups of the polymer have obvious vibration in the MIR band (8~13 μm). Thus, both FT-fabric and T-fabric have similar peak shapes in this band. Secondly, FT-fabric has microporosity of similar scale in the MIR band,

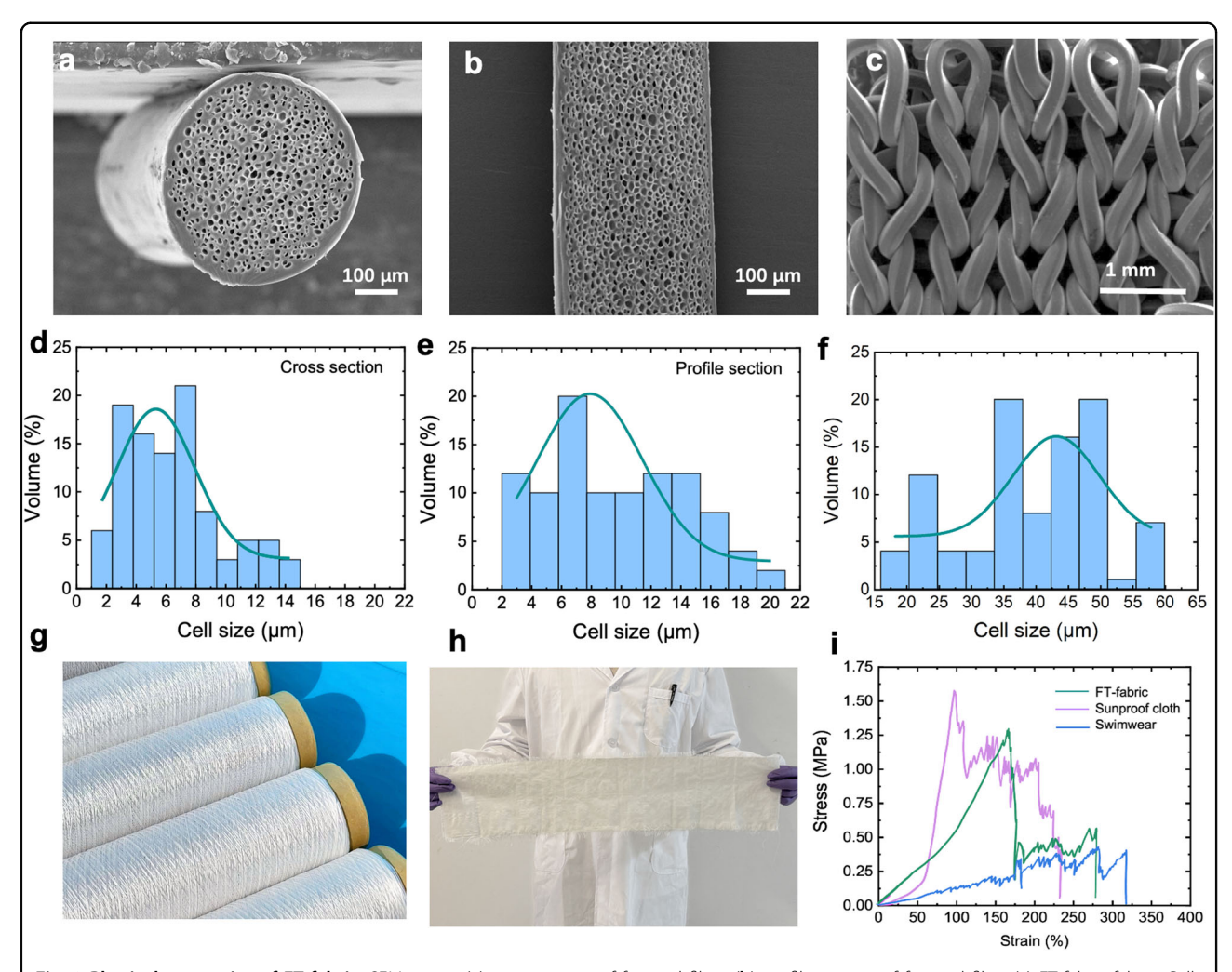


Fig. 2 Physical properties of FT-fabric. SEM image (a) cross-section of foamed fiber, (b) profile section of foamed fiber (c) FT-fabric fabric. Cell structure distribution. d Cross section of foamed fiber. e Profile section of foamed fiber (f) FT-fabric. g Optical photo of foamed fiber. h Optical photo of FT-fabric, sunproof cloth, and swimwear tensile stress-strain testing.

which further produces an interference effect, increases its emissivity and decreases its transmittance. In addition, Fig. 3d shows the ratio of emissivity and transmittance of FT-fabric in the MIR band. According to Kirchhoff's law, transmittance + reflectance + emissivity =1 (in the MIR band, the reflectance of FT-fabric can be almost considered to be 0), therefore, transmittance =1-emissivity. FT-fabric has an average transmittance of 27% over the entire 4–25 μ m region, indicating that it can transmit one-third of the body's radiant energy.

The net cooling power $(P_{\rm net})$ is calculated using a radiative cooling theoretical model⁴⁶, which is based on the measured data of nighttime and daytime reflectance spectra, and the net radiative cooling power of FT-fabric during daytime and nighttime are shown in Fig. 3e, f, respectively.

A cooling model was used to simulate and estimate the cooling power of FT-fabric, the net cooling power P_{net} can

be calculated by the following Eq. (1).

$$P_{net} = P_{rad} - P_{atm} - P_{sun} - P_{non-rad} \tag{1}$$

Where P_{rad} is the emitted thermal radiation from the FT-fabric, can be defined as Eq. (2).

$$P_{rad} = 2\pi \int_{0}^{\pi/2} \sin\theta \cos\theta d\theta \int_{0}^{\infty} \varepsilon_{m} I_{bb}(T_{f}) d\lambda \qquad (2)$$

Furthermore, P_{atm} indicates the absorbed thermal radiation from the atmosphere at the temperature T_{atm} , it can be calculated by Eq. (3).

$$P_{atm} = 2\pi \int_{0}^{\pi/2} \sin\theta \cos\theta \, d\theta \int_{0}^{\infty} \varepsilon_{atm} I_{bb}(T_{atm}) d\lambda$$
(3)

Where $I_{bb}(T)$ is the radiation intensity of black body, it can be calculated from Eq. (4), c is the speed of light (3 × 10⁸

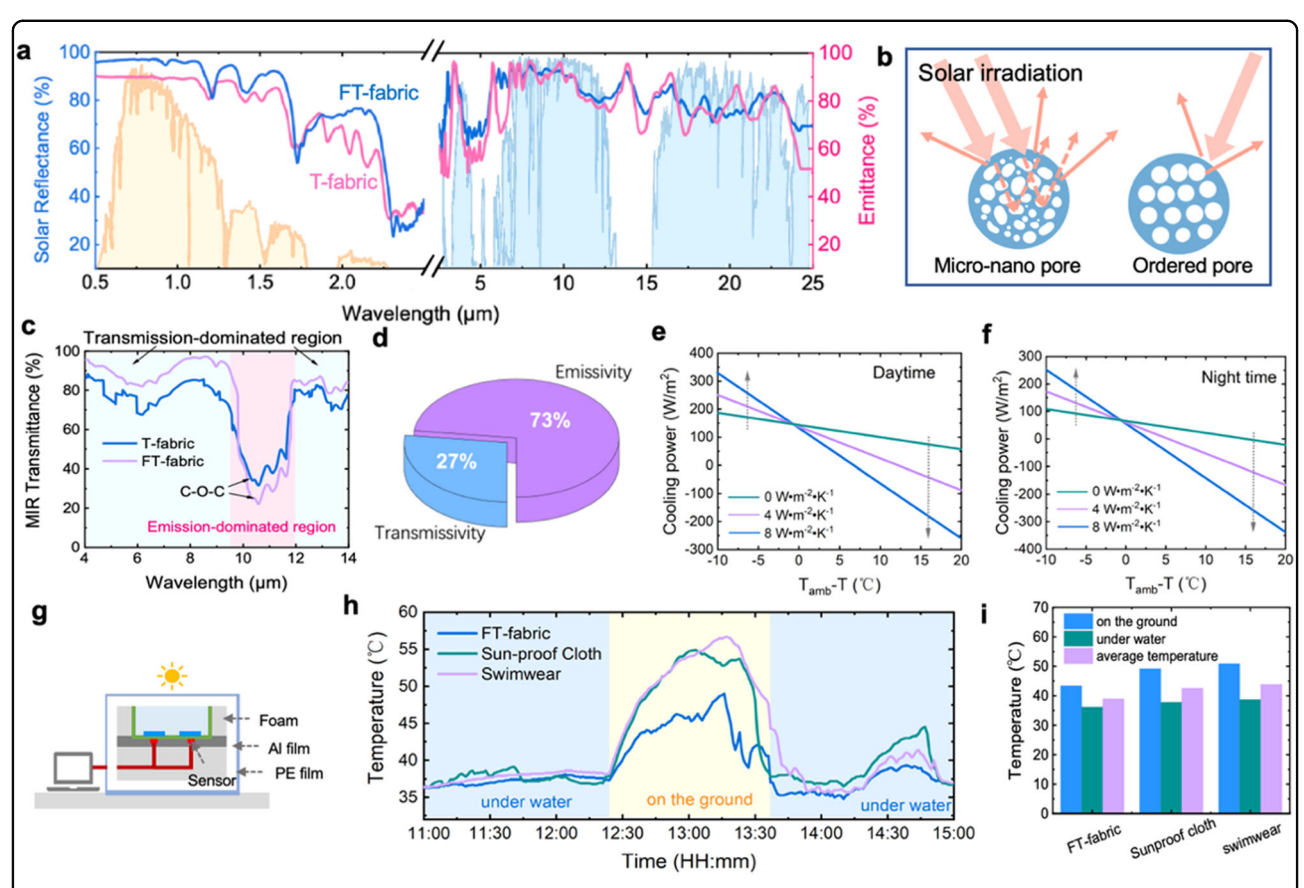


Fig. 3 Radiative cooling properties of FT-fabric. a Reflectance and emissivity testing of FT-fabric and T fabric. b Scattering mechanism of foamed fiber and traditional ordered foamed fiber. c FTIR-ATR tests for FT-fabric and T-fabric. d The emissivity and transmittance ratio of FT-fabric in the MIR band. Radiant cooling power (e) daytime (f) night time. g Schematic diagram of device for radiative cooling test. h FT-fabric, sunproof cloth and swimwear practical testing of radiative cooling (Data were recorded on August 5th in Guangzhou, China). i Average temperature change for FT-fabric, sunproof cloth and swimwear.

m s⁻¹), h is the reduced Planck constant (1.055 × 10⁻³⁴ J s), K_B is the Boltzmann constant (1.381 × 10⁻²³ J K⁻¹), and the λ is the wavelength, respectively.

$$I_{bb}(T) = \frac{4c^2l}{\lambda^5} \times \frac{1}{e^{\frac{lc}{\lambda K_B T}} - 1} \tag{4}$$

 $P_{non-rad}$ indicates the heat transfer by convection and conduction, it can be calculated by Eq. (5), where h is the heat transfer coefficient, T_{atm} is the atmosphere temperature, and T_f is the surface temperature of FT-fabric.

$$P_{non-rad} = h(T_{atm} - T_f) \tag{5}$$

The solar radiation intensity is provided by AM1.5(λ), and θ is taken as 0° because our test device is completely facing the sun. According to the result, the radiative cooling power of FT-fabric is higher at night than during

daytime, which is due to the fact that there is no direct solar irradiation at night, which reduces the energy input by a large amount. These results confirm the high radiative cooling power of FT-fabric.

In addition, we designed an experimental setup to verify the out-of-world cooling performance of FT-fabric on a sunny day in Guangzhou, China. the schematic of the experimental setup is shown in Fig. 3g, where the power density of the simulated skin is 100 W/m², the specific test procedures and details are shown in Fig. S2. The simulated skin covered with FT-fabric, sunproof cloth, and a swimming costume is exposed to the sun at the hottest time of the day (from 10:00 a.m. to 15:00 PM) the temperature variations in different scenarios are shown in Fig. 3h. Overall, the temperature changes of the three different textiles are relatively smooth when the materials are placed on the water surface, while the simulated skin temperature of the FT-fabric covered with the FT-fabric is significantly lower than that of the sunproof cloth and the swimming costume when it is on the ground. In Fig. 3i,

the average temperature FT-fabric is 39.2 °C, much lower than sunproof cloth (43.4 °C) and swimming costume (46.1 °C). We added the reflectivity of sunproof cloth and swimwear in Fig. S3. The results show that the sunproof cloth has a high reflectivity in the visible band, but the reflectivity in the near infrared has decreased significantly, which is because the main function of the sunproof cloth is to prevent UVA and UVB damage to the skin, and its action band is concentrated in the visible band. The reflectance of the swimwear is less than 70%, because the swimwear used in this test is the swimwear sold in the market, and has no sunscreen effect, so the reflectance is low.

Specifically, we tested the temperature changes of different textiles on water and on land, respectively. In Fig. 4a, b the temperature variations of simulated skin covered with FT-fabric, sunproof cloth and swimming costume on water and on land are shown, respectively. Figure 4c tests the variation of solar radiation intensity during its testing. In Fig. 4a, the temperature change of FT-fabric is relatively smooth compared to the other textiles, with no obvious peak temperature appearing. This is due to the low thermal conductivity of FT-fabric due to its porous structure, which can slow down the heat exchange and keep the internal temperature in a stable range while cooling down in the water. The average temperature change of sunproof cloth and swimwear is also lower in water than on the ground, but both are significantly higher than that of FT-fabric.

In addition, to demonstrate the cooling effect, we tested the surface temperature change of the moistened textiles by applying them to the human body and exposing them to the sun (Fig. 4e, f). Figure 4e shows the infrared images during the test, and it is evident that FTfabric clearly exhibits a lower surface temperature at the same solar radiation intensity. In Fig. 4f, we clearly see that the surface temperatures of the wetted fabrics are all about 25 °C at the beginning, while FT-fabric and sunproof cloth are the first to warm up with the change of the sun exposure time, which is mainly due to the fact that both textiles are hydrophobic and have less water absorption, so the water stained on their surfaces will evaporate quickly under the sun irradiation, resulting in the phenomenon of rapid warming. Swimwear, on the other hand, is more absorbent and has a higher water content, so the temperature change under sunlight is smaller.

The application of FT-fabric in buoyancy swimwear

The low density of the FT-fabric swimwear necessarily provides the appropriate buoyancy for the swimmers, thus ensuring the safety of the users, which gives the potential for large-scale commercialization of the FT-fabric. Meanwhile, the beneficial effects of the FT-fabric

swimwear in practical application scenarios are described, including the buoyancy quantitative data, air permeability and moisture permeability, quick-drying performance, and weathering resistance.

As shown in Fig. 5a, we tested the net buoyancy of the textiles using the drainage method according to ISO standard 12402-9:2006.51⁴⁷. Firstly, we measured and recorded the weight of the container completely filled with water, W_I , and the mass of the wetted textile, W_f . The wetted textile was immersed in the container and the glass lid was pressed until no air bubbles appeared, then the excess water was drained from the container and the outside of the container was wiped dry, at which point the weight of the entire container and the textile was W_2 . (All units are grams. The test was repeated more than three times for each sample).

The mass of the sample drained of water in the container is:

$$M_w = W_1 - (W_2 - W_f) (6)$$

Where $M_{\rm w}$ is the mass of the water that the sample flows away, W_I is the weight of the container after it is filled with water, W_2 is the weight of the container containing the water and the sample, and W_f is the average wet mass of the sample. This is then converted into units of volume by the following equation

$$V_f = \frac{M_w}{1000000} \tag{7}$$

where $M_{\rm w}$ is the mass of the water displaced by the sample (g) and V_f is the volume of the sample (m³).

Following Archimedes' principle⁴⁸, the net buoyant force of the samples is calculated as follows

$$F_{net} = \rho_f V_f g - mg \tag{8}$$

where F_{net} is the net buoyancy (*N*), ρ_f is the density of water ($\rho_f = 1000 \text{ kg/m}^3$), V_f is the volume of the sample in m³, g is the Earth's standard gravity ($g = 9.807 \text{ m/s}^2$), and m is the mass of the sample (kg). The mass of the sample can be measured with an electric balance.

Based on the test of the drained water method, we calculated the buoyancy of the same size ($10 \text{ cm} \times 10 \text{ cm}$) FT-fabric, sunproof cloth, and swimming costume as well as their densities (Fig. 5b). It can be seen that due to the ultra-low density of FT-fabric (0.62 g/cm^3), it is able to provide a buoyancy force of ~0.68 N. In order to quantitatively describe the role of FT-fabric swimwear in practical application scenarios, the surface area of human body

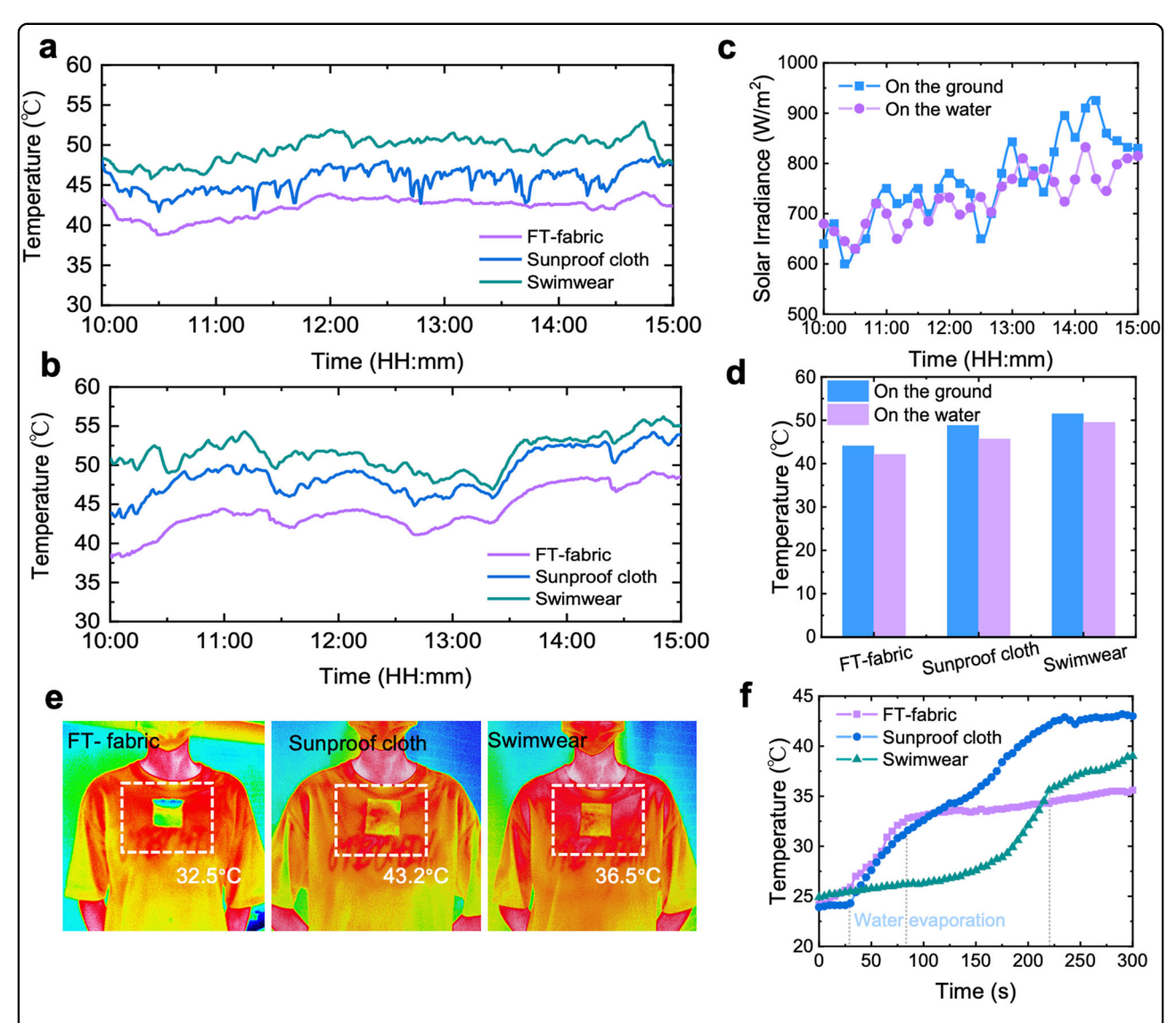


Fig. 4 Radiation cooling test of FT-fabric. The actual temperature of FT-fabric, sunproof cloth and swimwear is tested (a) on water and (b) on land (Data was recorded on August 6th in Guangzhou, China). c Changes in solar radiation during the actual temperature test of fabric, sunproof cloth and swimwear. d The average temperature of the actual temperature test for FT-fabric, sunproof cloth and swimwear. e Infrared images of wetted FT-fabric, sunproof cloth and bathing suit evaporation test. f Evaporation test results for FT-fabric, sunproof cloth and swimwear.

can be calculated by Stevenson formula:

$$S = 0.0061 * H + 0.0128 * W - 0.1529 \tag{9}$$

Where, S is the surface area of human body, m^2 . H is the height of human body, cm. W is the weight of human body, kg.

As can be seen from Fig. 5c, we have tested the buoyancy changes of FT-fabric and swimwear of different thicknesses. It can be seen that the buoyancy of FT-fabric increases significantly with the increase of thickness and is much higher than that of swimwear.

For example, a FT-fabric swimwear (wear area is 50% of the surface area of human body) can provide about 51.82 N of buoyancy for an adult woman (170 cm of height and 50 kg of weight), accounting for about 10% of body weight. This means that in a swimming scene dominated by safety and comfort, the FT-fabric swimwear provides users with significant safety features while balancing mobility (compared to the life-jacket with ultralow density). The sunproof cloth and swimming costume are both much denser than water, and, therefore, difficult to float on the water surface, and the calculated net buoyancy force is just less than 0.1 N, which makes it difficult to realize the buoyancy force provided.

As a wearable device, air permeability and moisture permeability are also key factors affecting its wearing comfort, so we tested the air permeability and moisture

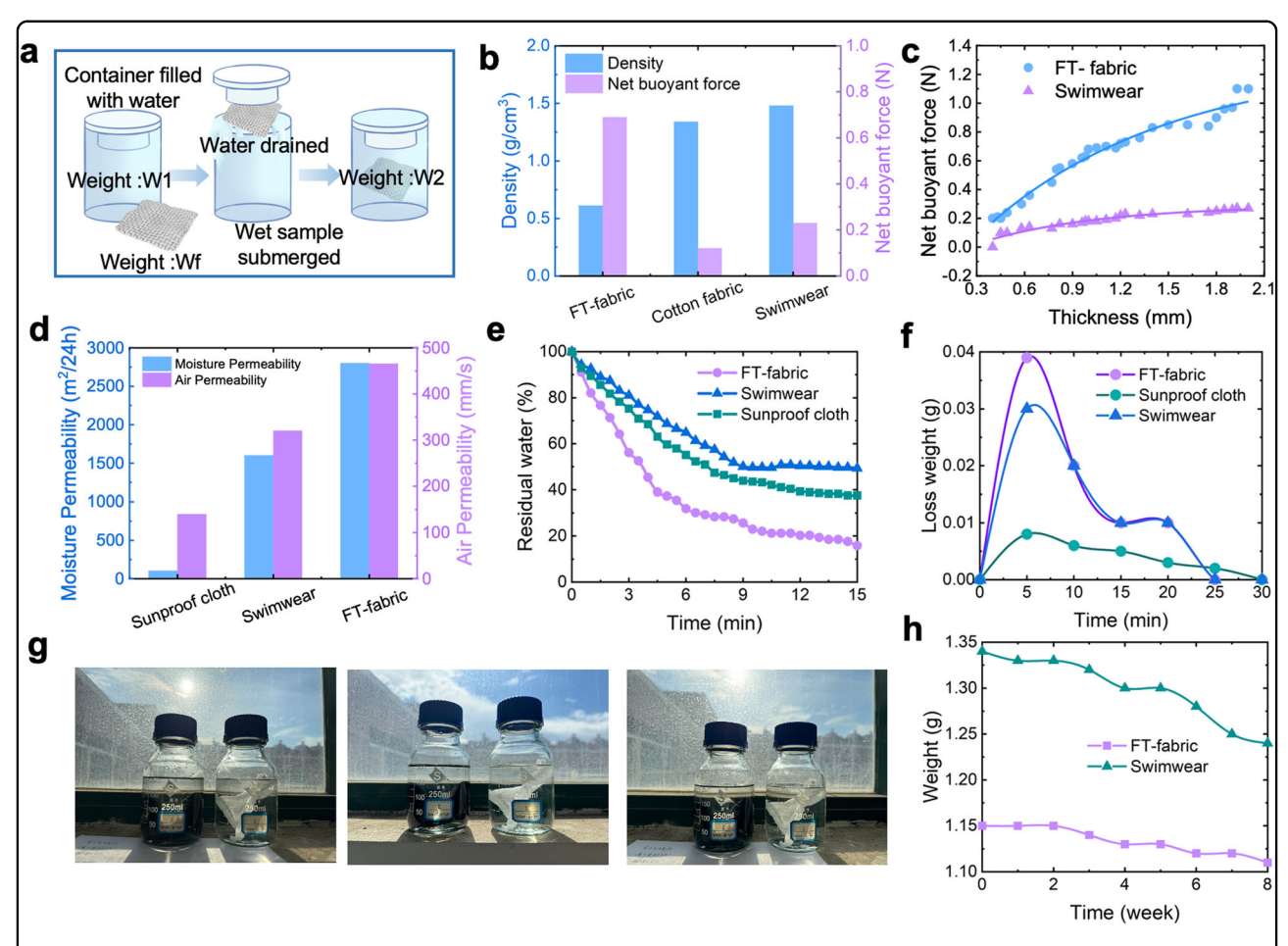


Fig. 5 Applicability testing of FT-fabric. a Schematic diagram of buoyancy test by drainage method. b FT-fabric, sunproof cloth and swimwear buoyancy and density testing. c The buoyancy of FT-fabric and swimwear varies with thickness. d FT-fabric, sunproof cloth and swimwear breathability and moisture permeability test. e Changes in residual water volume of moistened FT-fabric, sunproof cloth, and bathing suits under direct sun. f The amount of water evaporated from FT-fabric, sunproof cloth and swimwear. g FT-fabric and swimwear weather resistance testing. h Weight change of FT-fabric and swimwear soaked in seawater for 8 weeks.

permeability of three textiles in Fig. 5d. sunproof cloth often adopts a UV-resistant coating on the surface of polyester fabrics to achieve lower than the effect of solar radiation, and thus will inevitably sacrifice its air permeability and moisture permeability. FT-fabric, on the other hand, exhibits superb air permeability and moisture permeability, which makes it comfortable to wear in any scenario. In addition, the user's comfort after temporarily leaving the water is also worth considering, and this process strongly depends on the swimwear's excellent quick-drying performance. Figure 5e shows the variation of residual water content of fully wetted textiles under direct sunlight (solar radiation intensity of 897 W/m²). With the increase of sunlight exposure time, the residual water content of FT-fabric decreases rapidly to 20% in ~6 min and tends to stabilize, whereas the residual water content of sunproof cloth and swimming costume changes less. The residual water content of FT-fabric decreases rapidly, mainly due to the rapid decrease of water content of FT-fabric. The main reason for the rapid decrease in the residual water content of FT-fabric is that its superhydrophobic surface carries less initial water than other textiles after wetting in water, and therefore evaporates more quickly during drying (Fig. S5). We have measured the evaporation rate of FT-fabric, sunscreen clothing and swimwear according to fabric evaporation test standard GB/T21655.1-2008. It can be seen that the evaporation rate of FT-fabric also shows a high value under the same test conditions (Fig. 5f). Finally, because seawater contains substances such as sodium chloride, ammonia and iodine, it is crucial to have good weathering resistance. To test the weathering resistance of FT-fabric, we submerged the same area of FT-fabric purchased swimming costumes in seawater and left them outdoors for a period of 8 weeks, and recorded the changes in their quality on a weekly basis (Fig. 5g). From Fig. 5h, it can be seen that after

8 weeks of weathering test, the weight of FT-fabric decreased by $0.03\,\mathrm{g}$, while the swimming costume decreased by $0.11\,\mathrm{g}$, which proves that FT-fabric has good stability.

Conclusion

In conclusion, we have developed and validated a new type of functional garment through micro-extruded physical foaming technology. By introducing foaming technology into fiber preparation can solve the current problems of difficult weight reduction and functionality of fibers, and has a wide range of potential applications. Firstly, FT-fabric can effectively reflect near-infrared sunlight, thanks to the multi-level distribution pore strategy in the fiber. Secondly, since the FT-fabric can provide buoyancy, air permeability and moisture permeability, quick-drying performance, and weathering resistance, this brings security, comfort and movability to users in swimming scene. Finally, our fiber preparation process has the convenience of being manufactured on a large scale like currently common fibers. Our work will provide a generic strategy for designing micro- and nanostructured radiatively cooled textile materials and will be important for the future development of functional clothing.

Materials and method

Material

Thermoplastic Polyester Elastomer (TPU, 93 A) raw material granules, purchased from DuPont Company (USA). Nitrogen gas (purity of 99.9%), obtained from Guangqi Gas Company (China).

Preparation of foamed fiber

The micro-extrusion physical foaming process in this work uses $\rm N_2$ as blowing agent. The TPU filament was saturated at 25 MPa/30 °C for 24 h, and the content of the saturated mixed gas was 1.25 wt%. Then the saturated TPU filament was placed in a low-temperature environment of $\rm -15$ °C with aim to minimize the gas escape. A home-made micro-extruder was used to extrude the saturated filament with the nozzle temperature at 220 °C and feeding rate of about 4.5 m/min, and the foamed porous TPU fiber was heat-stretched at 100–120 °C with various stretching rates of 0.5–2.5 m/s.

Weaving of FT-fabric

The automatic rapier knitting machine (Sansi Machinery Co., Ltd.) was used for weaving, named as FT-fabric.

Material characterization

The morphology of foamed fiber, and bionic porous structure were characterized via a COXEM EM-30AX SEM. The specimens were quickly snapped or cut off in liquid nitrogen, glued to the sample stand with conductive glue, and then sprayed with gold on the surface. SEM was used to observe the surface, cross-section morphology, and radial morphology of foamed fibers. The moisture absorption, thermal conductivity and cooling processes of the samples were captured using thermocouples and a Nicolet 6700 Fourier Transform Infrared (FTIR) meter.

Spectral characterization

The spectral properties of the FT-fabric were characterized separately in the solar spectrum (0.3–2.5 $\mu m)$ and MIR (2.5–25 $\mu m)$ wavebands. The solar reflection and transmission spectra were recorded using an ultraviolet–visible–near-infrared spectrophotometer (Cary 7000, Agilent) and a FTIR spectrometer (INVENIO, Bruker) equipped with a gold integrating sphere (A562, Bruker) was used to measure the absorption–emission and transmission spectra.

Cooling measurements

The cooling effects of the different textiles were measured using the devices shown in Fig. 3g. Aluminum foil and foam in the test device were utilized to minimize the thermal impact from the surroundings, as in a method used in previous works. The thermocouples connected to a recorder were used to monitor the sample's temperature in real-time.

Buoyancy test

The true buoyancy of FT-fabric and swimsuit pairs was tested using the drainage method based on ISO standard 12402-9:2006.51, and the test diagram is shown in Fig. 5a.

Air permeability test

the test standard based on GB/T5453-1997 textile fabric breathability determination. According to the breathability standard of the textile, the applied pressure was 100 Pa, the applied area was 20 cm², the test temperature was 20 °C, the ambient humidity was 65%, and the air permeability of the fabric was measured ten times at different positions to take the average value.

Acknowledgements

The authors are grateful to the National Natural Science Foundation of China (52173053) and the Key-Area Research and Development Program of Guangdong Province (2023B0101010003) for funding this study.

Author contributions

W.Y. and Z.W. conceived the concept of this work. W.Y. Carried out all the experiments with the assistance of W.Z., H.H., W.Y., and Z.W. wrote the manuscript. All authors contributed to finalizing the manuscript.

Data availability

All data are available in the manuscript or the supplementary materials. Information requests should be directed to the corresponding author.

Competing interests

The authors declare no competing interests.

Ethics approval and consent to participate

We confirm that all methods used in this work are carried out in accordance with relevant guidelines and regulations. No live animals were used in this work, and the informed consent of all participants has been obtained. The identifiable images from human study participants involved in this work have all received written informed consent for their release.

Publisher's note

Springer Nature remains neutral with regard to jurisdictional claims in published maps and institutional affiliations.

Supplementary information The online version contains supplementary material available at https://doi.org/10.1038/s41427-025-00586-8.

Received: 28 August 2024 Revised: 4 December 2024 Accepted: 19 December 2024

Published online: 28 February 2025

References

- Zhai, W., Jiang, J. & Park, C. B. A review on physical foaming of thermoplastic and vulcanized elastomers. *Polym. Rev.* 62, 95–141 (2022).
- Zhai, W. & Jiang, J. Fundamental issues for batch foaming of thermoplastic elastomers with supercritical fluids. *Acta Polym. Sin.* 55, 369–395 (2024).
- Jiang, J., Liu, H., Tian, F., Chen, B. & Zhai, W. Progress on research and applications of polymeric foams and porous functional materials (in Chinese). *Chin. Sci. Bull.* 69, 2964–2977 (2024).
- Wu, G. et al. A review of thermoplastic polymer foams for functional applications. J. Mater. Sci. 56, 11579–11604 (2021).
- Jiang, S., Agarwal, S. & Greiner, A. Low-density open cellular sponges as functional materials. *Angew. Chem. Int. Ed.* 56, 15520–15538 (2017).
- Li, D. et al. High-expansion open-cell polylactide foams prepared by microcellular foaming based on stereocomplexation mechanism with outstanding oil-water separation. *Polymers* 15, 1984 (2023).
- Sahoo, M. K. & Mandal, A. Design and analysis of three-dimensional foams: a review. Arch. Comput. Method Eng. 113, 1–29 (2024).
- Zhou, Y., Tian, Y. & Zhang, M. Technical development and application of supercritical CO2 foaming technology in PCL foam production. Sci. Rep. 14, 6825 (2024).
- Zhou, Y., Tian, Y. & Peng, X. Applications and challenges of supercritical foaming technology. *Polymers* 15, 402 (2023).
- Cuadra-Rodriguez, D., Barroso-Solares, S. & Pinto, J. Advanced nanocellular foams: perspectives on the current knowledge and challenges. *Nanomaterials* 11. 621 (2021).
- Azdast, T. & Hasanzadeh, R. Increasing cell density/decreasing cell size to produce microcellular and nanocellular thermoplastic foams: a review. J. Cell Plast. 57, 769–797 (2021).
- Jiang, J. et al. Evolution of ordered structure of TPU in high-elastic state and their influences on the autoclave foaming of TPU and inter-bead bonding of expanded TPU beads. *Polymer* 228, 123872 (2021).
- Jiang, J. et al. Microstructure development of PEBA and its impact on autoclave foaming behavior and iner-bead bonding of EPEBA beads. *Polymer* 256, 125244 (2022).
- Ge, C., Wang, S., Zheng, W. & Zhai, W. Preparation of microcellular thermoplastic polyurethane (TPU) foam and its tensile property. *Polym. Eng. Sci.* 58, 158–166 (2018).
- Ge, C. & Zhai, W. Cellular thermoplastic polyurethane thin film: Preparation, elasticity, and thermal insulation performance. *Ind. Eng. Chem. Res.* 57, 4688–4696 (2018).
- Jiang, J., Zheng, H., Liu, H. & Zhai, W. Tunable cell structure and mechanism in porous thermoplastic polyurethane micro-film fabricated by a diffusion-restricted physical foaming process. J. Supercrit. Fluids 171, 105205 (2021).

- Li, M., Jiang, J., Hu, B. & Zhai, W. Fused deposition modeling of hierarchical porous polyetherimide assisted by an in-situ CO₂ foaming technology. Compos. Sci. Technol. 200, 108454 (2020).
- Zhai, W., Hu, B., Li, M., Jiang, J. & Zhou, M. Dimensional accuracy control and compressive property of microcellular polyetherimide honeycomb foams manufactured by an situ foaming fused deposition modeling technology. *Adv. Eng. Mater.* 23, 2001449 (2021).
- Chen, B. et al. Controlling the crystal morphology of high-hardness TPU through two pre-crystallization processes and its impact on physical foaming behavior. *Polymer* 305, 127172 (2024).
- Tian, F., Huang, H., Li, Y. & Zhai, W. Fabrication of soft biodegradable foam with improved shrinkage resistance and thermal stability. *Materials* 17, 3712 (2024).
- Jiang, J., Feng, W., Zhao, D. & Zhai, W. Poly (ether imide)/epoxy foam composites with a microcellular structure and ultralow density: Bead foam fabrication, compression molding, mechanical properties, thermal stability, and flame-retardant properties. ACS Omega 5, 26784–25797 (2020).
- Zhang, C. et al. Wood-cellulose-fiber-based functional materials for triboelectric nanogenerators. Nano Energy 81, 105637 (2021).
- Abbood, I. S., aldeen, Odaa, S., Hasan, K. F. & Jasim, M. A. Properties evaluation of fiber reinforced polymers and their constituent materials used in structures-a review. *Mater. Today Proc.* 43, 1003–1008 (2021).
- Zhu, C., Wu, J., Yan, J. & Liu, X. Advanced fiber materials for wearable electronics. Adv. Fiber Mater. 5, 12–35 (2023).
- Shen, Y. et al. Review on fiber-based thermoelectrics: materials, devices, and textiles. Adv. Fiber Mater. 5, 1105–1140 (2023).
- Chen, C. et al. Functional fiber materials to smart fiber devices. Chem. Rev. 123, 613–662 (2022).
- Zhou, M. et al. Porous polyetherimide fiber fabricated by a facile microextrusion foaming for high temperature thermal insulation. J. CO2 Util. 65, 102247 (2022).
- Sheng, Z. et al. The rising aerogel fibers: status, challenges, and opportunities. Adv. Sci. 10, 2205762 (2023).
- Huang, Y., Xiao, C., Huang, Q., Liu, H. & Zhao, J. Progress on polymeric hollow fiber membrane preparation technique from the perspective of green and sustainable development. Chem. Eng. J. 403, 126295 (2021).
- Huang, C. & Thomas, N. L. Fabrication of porous fibers via electrospinning: strategies and applications. *Polym. Rev.* 60, 595–647 (2020).
- Ge, P., Wang, S., Zhang, J. & Yang, B. Micro-/nanostructures meet anisotropic wetting: from preparation methods to applications. *Mater. Horiz.* 7, 2566–2595 (2020).
- Shao, G., Hanaor, D. A., Shen, X. & Gurlo, A. Freeze casting: from low-dimensional building blocks to aligned porous structures—a review of novel materials, methods, and applications. *Adv. Mater.* 32, 1907176 (2020).
- Dai, C., Zhang, C., Huang, W., Chang, K. & Lee, L. Thermoplastic polyurethane microcellular fibers via supercritical carbon dioxide based extrusion foaming. *Poly. Eng. Sci.* 53, 2360–2369 (2013).
- 34. Li, M. et al. Microextrusion foaming of polyetheretherketone fiber: mechanical and thermal insulation properties. *Adv. Eng. Mater.* **24**, 2101110 (2022).
- Zhang, F., Si, Y., Yu, J. & Ding, B. Electrospun porous engineered nanofiber materials: a versatile medium for energy and environmental applications. *Chem. Eng. J.* 456, 140989 (2023).
- Shahbazi, M. A., Ghalkhani, M. & Maleki, H. Directional freeze-casting: a bioinspired method to assemble multifunctional aligned porous structures for advanced applications. *Adv. Eng. Mater.* 22, 2000033 (2020).
- Yang, X. & Berglund, L. A. Structural and ecofriendly holocellulose materials from wood: microscale fibers and nanoscale fibrils. Adv. Mater. 33, 2001118 (2021).
- 38. Chen, W. Y., Shi, X. L., Zou, J. & Chen, Z. G. Wearable fiber-based thermoelectrics from materials to applications. *Nano Energy* **81**, 105684 (2021).
- Liu, Z. et al. Functionalized fiber-based strain sensors: pathway to nextgeneration wearable electronics. *Nanomicro Lett.* 14, 61 (2022).
- Xiong, J., Chen, J. & Lee, P. S. Functional fibers and fabrics for soft robotics, wearables, and human–robot interface. Adv. Mater. 33, 2002640 (2021).
- 41. Xiao, R., Yu, G., Xu, B. B., Wang, N. & Liu, X. Fiber surface/interfacial engineering on wearable electronics. *Small* **17**, 2102903 (2021).
- Lu, J. T. & Ilyas, E. An overview of ultraviolet-protective clothing. Cureus 14, 7 (2022).
- Azad, S. S. et al. Stability enhancement of perovskite solar cells using multifunctional inorganic materials with UV protective, self-cleaning, and high wear resistance properties. Sci. Rep. 14, 6466 (2024).

- 44. Zhai, H., Fan, D. & Li, Q. Dynamic radiation regulations for thermal comfort. *Nano Energy* **100**, 107435 (2022).
- 45. Dorodnyy, A., Smajic, J. & Leuthold, J. Mie scattering for photonic devices. *Laser Photonics Rev.* **17**, 2300055 (2023).
- 46. Yu, X., Chan, J. & Chen, C. Review of radiative cooling materials: performance evaluation and design approaches. *Nano Energy* **88**, 106259 (2021).
- 47. Li, N. W., Ho, C. P., Yick, K. L. & Zhou, J. Y. Influence of inlaid material, yarn and knitted structure on the net buoyant force and mechanical properties of inlaid knitted fabric for buoyant swimwear. *Text. Res. J.* **91**, 1452–1466 (2021).
- 48. Cavazzini, G. Archimedes' principle and the concept of gravitation. *Appl. Phys. Rev.* 11, 9 (2019).